THE JOURNAL OF PHYSICAL CHEMISTRY A

Article

Cite This: J. Phys. Chem. A 2019, 123, 4149−4157

pubs.acs.org/JPCA

Gas-Phase Infrared Ion Spectroscopy Characterization of Cu(II/I)Cyclam and Cu(II/I)2,2′-Bipyridine Redox Pairs

Musleh Uddin Munshi,[†] Jonathan Martens,[†] Giel Berden,[†] and Jos Oomens*[,†,‡]

[†]Radboud University, Institute for Molecules and Materials, FELIX Laboratory, Toernooiveld 7, 6525 ED Nijmegen, The Netherlands

[‡]University of Amsterdam, Science Park 904, 1098 XH Amsterdam, The Netherlands

Supporting Information

ABSTRACT: We report the fingerprint IR spectra of mass-isolated gaseous coordination complexes of 2,2′-bipyridine (bpy) and 1,4,8,11-tetra-azacyclotetradecane (cyclam) with a copper ion in its I and II oxidation states. Experiments are carried out in a quadrupole ion trap (QIT) mass spectrometer coupled to the FELIX infrared free-electron laser. Dications are prepared using electrospray ionization (ESI), while monocations are generated by charge reduction of the dication using electron transfer-reduction (ETR) in the QIT. Interestingly, $[Cu(bpy)_2]^+$ can also be generated directly using ESI, so that its geometries as produced from ETR and ESI can be compared. The effects of charge reduction on the IR spectra are investigated by comparing the experimental spectra with the IR spectra modeled by density functional theory. Reduction of Cu(II) to the closed-shell Cu(I) ion retains the square-planar geometry of the Cu−cyclam complex. In contrast, for the bis−bpy complex with Cu, charge reduction induces a conversion from a near-square-planar to a tetrahedral geometry. The geometry of $[Cu(bpy)_2]^+$ is identical to that of the complex generated directly from ESI as a native structure, which indicates that the ETR product ion thermalizes. For $[Cu(cyclam)]^+$, however, the square-planar geometry of the 2+ complex is retained upon charge reduction, although a (distorted) tetrahedral geometry was predicted to be lower in energy. These differences are attributed to different barriers to rearrangement.

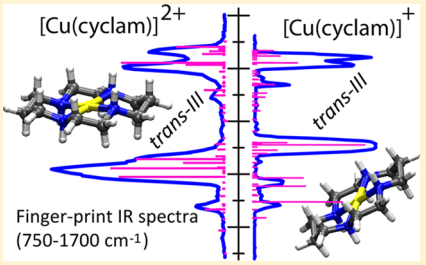

1. INTRODUCTION

Wavelength tunable infrared lasers coupled with various ion storage mass spectrometers have become invaluable instruments in ion chemistry.[1−8] Ion spectroscopy has enabled the routine recording of the IR spectra of mass-selected ions, from which accurate structural information can be derived. Quadrupole ion trap (QIT) mass spectrometers form versatile platforms for ion spectroscopy, offering multistage ion chemistry manipulation and analyses, such as collision-induced dissociation. Our group has recently constructed an ion spectroscopy platform[9] that allows for the spectroscopic investigation of product ions from ion/ion reactions.[10−13] These include product ions of electron transfer dissociation (ETD),[14−16] but also of electron transfer reduction (ETR),[17] i.e., charge reduction without further dissociation, sometimes dubbed ETnoD. We recently demonstrated that the geometry of the Ni(cyclam) coordination complex remains the same and intact (trans-III, see Scheme 1) upon gas-phase charge reduction of Ni^{2+}(cyclam) to Ni^{+}(cyclam).[17] Both members of this redox pair were spectroscopically probed in complete isolation employing IR ion spectroscopy, and structural characterization was aided by density functional theory (DFT) calculations.

Here, we further investigate this method to spectroscopically probe the two members of the metal−ligand redox pairs. For the present study, we choose Cu(II/I) ion as the metal center. Depending on the nature of the ligand, copper has an interesting property that both members of the redox pair can be generated directly by electrospray ionization (ESI), in contrast to most other first-row transition metals. This enables us to compare the spectra of 1+ coordination complexes generated both by ESI directly and by gas-phase ETR from the 2+ complex. In the choice of ligands, we have opted for a cyclic (cyclam) as well as a noncyclic (bpy) ligand; both ligands form

Scheme 1. $Cu(bpy)_2$ Complex (left) and Five Diastereomers of the Coordination Complex of Cu and Cyclam[a]

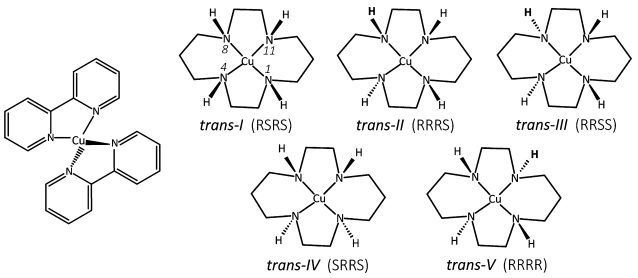

[a]The Cahn−Ingold−Prelog *R*/*S* chirality of each of the nitrogen centers is indicated in the order 1, 4, 8, 11 (atom numbering indicated for trans-I).

Received: January 25, 2019
Revised: April 25, 2019
Published: April 25, 2019

DOI: 10.1021/acs.jpca.9b00793
J. Phys. Chem. A 2019, 123, 4149−4157

tetradentate coordination complexes with Cu: bpy as a bis-complex and cyclam as a monocomplex. The complexation of cyclam with transition-metal ions has been studied,[18] but relatively little information is available about the coordination in the gas phase. Note that although the isolated cyclam molecule is not chiral, coordination of the nitrogen atoms to a metal center induces stereoisomerism. Five distinct diastereomers referred to as trans-I through trans-V are possible, related to the relative orientation of the four N−H bonds, see Scheme 1. In a previous paper,[17] we have shown that complexes of Ni(II) and Ni(I) with cyclam form only the trans-III diastereomer, which is consistent with the solution stereochemistry for Ni(II)-cyclam, although trans-I and trans-III were reported to coexist in a solution.[18]

Macrocyclic saturated tetra-amines generally have high affinity to form stable metal−ligand coordination complexes in a solution.[19,20] In particular, cyclam is known to form square-planar tetradentate complexes with Co(II), Ni(II), and Cu(II). Changes in the length of the alkyl chains connecting the N-atoms affect the structure and the spin state of the complexes in the solution[21,22] and in the solid state,[21] which is ascribed to steric hindrance effects as confirmed by UV−vis absorption spectroscopy in the solution.[23] Methyl derivatives of cyclam (such as 5,7,7,12,14,14-hexamethyl-1,4,8,11-tetraazacyclotetradecane) have also been reported to form stable complexes with Cu(II),[19] and coordination of N-tetraalkylated cyclam ligands with 3d transition metals have been reported to form trans-I complexes in the solution.[24] From a broader perspective, a significant fraction of enzymes possess a metal ion as a cofactor at their active sites, and their catalytic action often involves shuttling between oxidation states of the metal ion.[25,26] Copper-containing proteins are abundant, including for instance cytochrome oxidase, laccase oxidases, superoxidedismutases, (di)oxygenases, nitrite reductase, and N_2O reductase. Model metal−peptide complexes have been studied extensively[27,28] in the gas phase, including studies employing ion spectroscopy.[29−31] For example, both Ni(II) and Cu(II) have been shown to form low-spin square-planar geometries with tetraglycine having structures that are very similar to each other.[30]

In both oxidation states, Cu ions have similar ionic radii: 0.74 Å for Cu(I) versus 0.71 Å for Cu(II) in a four-coordination environment, where they form tetrahedral and square-planar coordination geometries, respectively.[19,32] Intrinsically, the main distinction between Cu(II) and Cu(I) is the d^9 electronic configuration of the former versus the closed-shell d^{10} configuration of the latter. Jahn−Teller distortion in Cu(II) complexes induces axial elongation of octahedral geometries forming square-pyramidal or square-planar geometries, whereas Cu(I) shows structural flexibility taking advantage of the low charge.[33,34]

2. EXPERIMENTAL SECTION

Experiments have been carried out in a modified QIT MS (Bruker AmaZon Speed ETD, Bremen, Germany) that has been described in detail elsewhere.[9,35] The modifications mainly involve optical access to the trapped ion cloud, enabling us to record the IR multiple-photon dissociation (IRMPD) spectra of mass isolated ions.

Coordination complexes of Cu^{2+} with the tetradentate cyclam ligand as well as the bis-complex with bpy (Cu^{2+}(cyclam) and $Cu^{2+}(bpy)_2$) were generated via electrospray ionization (ESI), using equimolar solutions (1 μM) of $CuSO_4$ and cyclam or bpy in 1:1 MeOH/H_2O. The singly charged Cu^+(cyclam) and $Cu^+(bpy)_2$ were generated by charge reduction using the electron-transfer dissociation (ETD) option of the QIT MS. The fluoranthene radical anion acts as a reducing agent in an ion−ion reaction with the mass-isolated dicationic complexes inside the ion trap. The fluoranthene radical anions are produced in a negative chemical ionization source[35,36] and transferred to the trap, where they undergo electron-transfer reaction. A reaction time of approximately 200−250 ms is found to yield the maximum number of charge-reduced ions for these complexes, while minimizing the number of ETD induced fragment ions. Singly charged Cu−bpy_2 complexes were also produced directly from the ESI source (even when using a Cu(II) salt, which is not uncommon[37]), but this was not possible for cyclam. We qualitatively attribute this difference to the hard/soft acid/base effects,[38] where the Cu^+ ion, a soft Lewis acid, coordinates more favorably with the soft Lewis basic pyridine N-atoms of bpy than with the hard Lewis-basic alkyl-amine N-atoms of cyclam.

We also investigate the IRMPD spectra of Cu^{2+}(cyclam) ions recorded in a Fourier Transform Ion Cyclotron Resonance (FTICR) MS, which has been described in detail elsewhere.[2,39] For this instrument, solutions of approximately 1 mM cyclam with Cu^{2+} in a 1:1 MeOH/H_2O were used. An advantage of the FT-ICR MS is that no helium buffer gas is used inside the ICR cell, which avoids collisional cooling of the complexes during IR activation by FEL, leading to a more efficient IRMPD (especially important for strongly bound complexes) and thus revealing additional weaker features in the IR spectra that escape observation in the QIT MS.[9] The FTICR MS instrument does not have the possibility to reduce the charge of the dications, so the IR spectra of Cu^+(cyclam) cannot be recorded on this setup.

To record the IRMPD spectra in the range from 500 to 1700 cm^{-1} in the QIT MS, mass-selected (m/z) ions are irradiated with 4−20 macropulses from the free electron laser FELIX.[9] About 6 μs long macropulses have energies up to 100 mJ and are produced at a 10 Hz repetition rate. When the IR frequency of the laser matches one of the vibrational absorption frequencies of the trapped ions, multiple photons are absorbed, increasing the internal energy of the ions and leading to unimolecular dissociation commonly via the minimum-energy channel. A series of mass spectra is saved while varying the IR wavelength, so an IR spectrum can be reconstructed by plotting the fragmentation yield (yield = $\sum$(fragment ions)/$\sum$(precursor + fragment ions)) at each laser wavelength.[1,40] Mass spectra are taken at every 3 cm^{-1} step of the laser frequency with 3−6 averages. The fragmentation yield is corrected linearly for the frequency-dependent laser pulse energy, and the frequencies are calibrated using a grating spectrometer.

The IRMPD experiment in the FTICR MS proceeds in an analogous fashion; however, the ions are additionally irradiated for 20 ms by the output of a continuous-wave CO_2 laser (10.6 μm, 30 W) directly after each FEL pulse to enhance the extent of dissociation.[41]

2.1. Theoretical Modeling. Quantum-chemical calculations are performed using density functional theory (DFT) to assist in structural and vibrational normal-mode assignments using the Gaussian 09 revision D01 code.[42] B3LYP[43−45] and UB3LYP levels of theory are employed for closed-shell (Cu^+) and open-shell (Cu^{2+}) systems, respectively. The 6-31+

DOI: 10.1021/acs.jpca.9b00793
J. Phys. Chem. A 2019, 123, 4149−4157

+G(d,p) basis set was used on all atoms including the Cu atom. No symmetry constraints are imposed. Cu^{2+} complexes have doublet multiplicity, and spin contamination was negligible for these systems. Single-point MP2/6-311+G(d,p) calculations were performed on the optimized B3LYP geometries to refine relative energies.

Harmonic IR frequencies are computed for the optimized geometries, and the frequencies are scaled by a factor of 0.975, which was reported to give the best match for various IRMPD spectra,[14,46] including those of Ni-cyclam ions,[17] to compensate for anharmonicity and basis set incompleteness. Computed IR frequencies are convoluted with a 15 cm^{-1} full width at half-maximum Gaussian line-shape function for direct comparison with the experimental spectra.

3. RESULTS AND DISCUSSION

3.1. Mass Spectra of $[Cu(bpy)_2]^{2+/+}$ Redox Pair. Figure 1a shows the ESI mass spectrum of a doubly charged

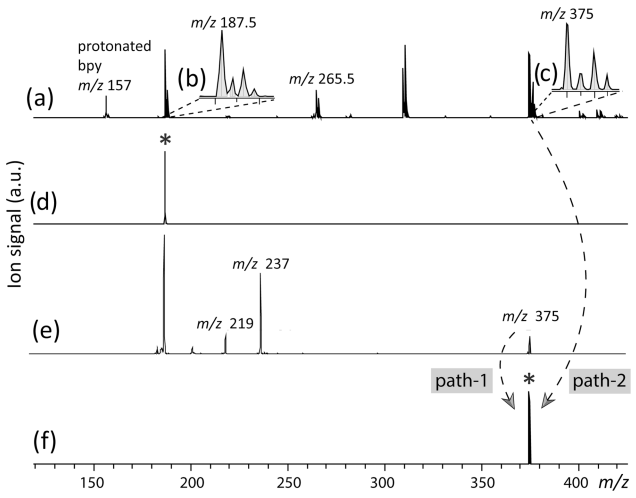

Figure 1. (a) ESI mass spectrum generated from a solution containing bpy and copper(II) sulfate, (b) the isotope distribution of the $[Cu(bpy)_2]^{2+}$ ion with the ^{63}Cu monoisotopic peak at m/z 187.5, and (c) $[^{63}Cu(bpy)_2]^{+}$ with its monoisotopic peak at m/z 375. (d) Isotope-selective mass isolation of the $[^{63}Cu(bpy)_2]^{2+}$ ion. (e) ETR reaction of isolated monoisotopic $[Cu(bpy)_2]^{2+}$, which generates a mass peak corresponding to the formation of the charge-reduced $[Cu(bpy)_2]^{+}$ ion at m/z 375. ETR-induced fragments are also observed: $[Cu(bpy)]^{+}$ at m/z 219 and the water adduct of this ion at m/z 237. (f) Isolation of the charge-reduced $[Cu(bpy)_2]^{+}$ ion (m/z 375) from the ETR mass spectrum (path 1) and from direct ESI MS (path 2). Members of the redox pair are indicated with a black star (d, f).

$[Cu(bpy)_2]^{2+}$ ion. The isotope pattern with the main peak at m/z 187.5 in the inset (b) is in agreement with the charge and stoichiometry of this complex. The ion at m/z 265.5 is attributed to the $[Cu(bpy)_3]^{2+}$ complex. In addition, the singly charged $[Cu(bpy)_2]^{+}$ ion is also observed in the MS, confirmed by its characteristic isotope pattern at m/z 375 (values are given for the monoisotopic peak, see panel c). In panel d, the $[^{63}Cu(bpy)_2]^{2+}$ ion is mass-isolated and used for (i) IRMPD spectroscopic measurements and (ii) charge reduction by ETR.

The IRMPD spectrum of the isolated $[Cu(bpy)_2]^{2+}$ ion (Figure 2a) is recorded to monitor the IR-induced photofragments at m/z 157, corresponding to protonated bpy. The

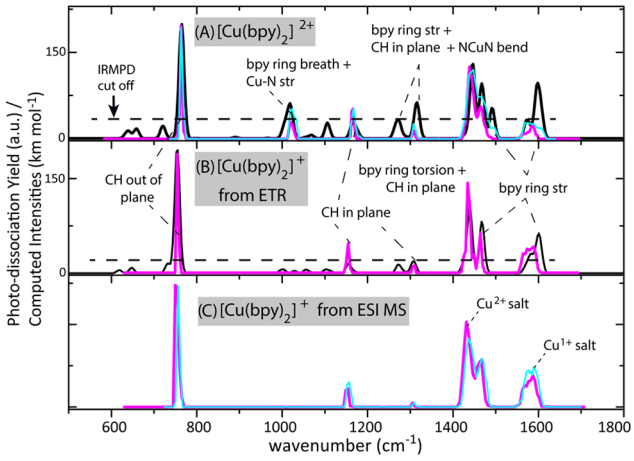

Figure 2. Experimental IRMPD spectra (magenta trace) of (a) $[Cu(bpy)_2]^{2+}$ and (b) $[Cu(bpy)_2]^{+}$ generated using ETR and (c) $[Cu(bpy)_2]^{+}$ generated directly from ESI. The cyan traces represent spectra obtained with a Cu(I) salt (Cu-acetate) in the ESI solution, and the magenta traces are obtained with a Cu(II) salt ($CuSO_4$). IRMPD spectra of $[Cu(bpy)_2]^{+}$ from all three sources appear to be identical (panels b and c). Both $[Cu(bpy)_2]^{2+}$ and $[Cu(bpy)_2]^{+}$ were irradiated with 4 macro pulses of the FEL to record their IRMPD spectra. Experimental spectra are overlaid with the theoretical linear IR spectra (black traces) for comparison. Their approximate IR mode descriptions are indicated. The horizontal dotted line indicates an apparent cutoff; bands with computed intensities below these levels are not observed in the experimental IRMPD spectrum, presumably due to the relatively high dissociation threshold of this complex. Such effects have been described in the literature.[5,9,48,49]

complementary ion appears at m/z 236 as a water adduct, $[Cu(bpy{-}H)(H_2O)]^{+}$, due to the relatively high background pressure in the QIT. In addition, the $[Cu(bpy)]^{+}$ ion is also produced at m/z 219 by loss of a neutral bpy unit. These $[Cu(bpy)]^{+}$ ions also form water adducts (m/z 237).

In a separate experiment, charge-reduced $[Cu(bpy)_2]^{+}$ ions are generated by charge reduction of the mass-isolated dication at m/z 187.5 using ETR (Figure 1e). In addition to the ETR product ion at m/z 375, ETR-induced fragments are also observed (m/z 219 and 237) due to the energy released in the charge recombination (electron transfer dissociation, ETD).[17,35,47] The intact charge-reduced ions are mass isolated (Figure 1f, path 1) to record their IRMPD spectrum, shown in Figure 2b. The same charge-reduced ions are also isolated directly from the ESI MS (Figure 1f, path 2), and their IRMPD spectrum was recorded separately (Figure 2c). During the IRMPD scan of the $[Cu(bpy)_2]^{+}$ ions formed either via path 1 or 2, IR-induced photofragments are formed at m/z 219 and 237, consistent with the collision-induced dissociation and ETD product ions (Figure 1e).

3.2. IR Spectra and Structural Assignments. The experimental IRMPD spectra of $[Cu(bpy)_2]^{+}$ obtained from ETR and from ESI directly as well as that of $[Cu(bpy)_2]^{2+}$ are shown in Figure 2. Experimental spectra are compared with theoretical linear IR spectra (black traces) of the two members of the redox pair. Panel a shows the IRMPD spectra of the doubly charged $[Cu(bpy)_2]^{2+}$ ion using ESI solutions containing either a Cu(II) or a Cu(I) salt ($CuSO_4$ or Cu[acetate]); the two spectra are nearly identical. Panel b shows the IRMPD spectrum of the charge-reduced ion, where the ions are generated from the dication using ETR (path 1 in Figure 1). In panel c, the IRMPD spectrum of the same singly

DOI: 10.1021/acs.jpca.9b00793
J. Phys. Chem. A 2019, 123, 4149−4157

charged ion is shown, but now isolated directly from the ESI MS (path 2 in Figure 1); both Cu(II) and Cu(I) salts were used again, but only insignificant differences in the resulting spectra were observed. Moreover, the IRMPD spectra of the charge-reduced ions in panels b and c are nearly identical, which indicates that the coordination geometries are the same whether the ion is generated through gas-phase charge reduction from the dication or directly extracted as a 1+ ion from the ion source.

The IR spectra for the singly and doubly charged ions are relatively similar except for an additional IR band at 1020 cm^{-1} for the dication. Also, slight shifts in the IR band positions are observed, which suggest small differences in the structures of the mono- and dications. Theoretical spectra reasonably reproduce all observed IRMPD bands for both members of the redox pair in terms of their band position; relative intensities are also in reasonable agreement. The optimized geometries confirm the tetradentate coordination to the metal center and are best characterized as distorted square-planar for the dication and tetrahedral for the monocation (vide infra).

The dominant IRMPD band for the dication is observed at 764 cm^{-1}, as correctly predicted by the computation at 766 cm^{-1}, and has primarily C−H out-of-plane bending character. The band observed at 1020 cm^{-1}, which is diagnostic for the dication, is correctly predicted at 1019 cm^{-1} and is attributed to the bpy ring breathing coupled with Cu−N stretching. The band observed and predicted at 1167 cm^{-1} is due to the C−H in-plane bending. The low-intensity IRMPD band at 1307 cm^{-1} is slightly blue-shifted in the calculation at 1319 cm^{-1} and has combined bpy-ring stretching, C−H in-plane bending, and N−Cu−N bending character. The IR bands observed between 1400 and 1500 cm^{-1} are also well predicted and are due to C−C, C−N stretching of the bpy ring with the C−H in-plane bending. The highest-frequency bands observed close to 1600 cm^{-1} are predominantly due to ring CC and NC stretching, typical for nitrogen heterocyclic species.

Generally, the observed intensities are in good overall agreement with the prediction, although theory predicts additional low-intensity bands that are not observed in the experiment for the dication. Even at higher FEL pulse energies, no additional bands were observed in the 1000−1400 cm^{-1} range (see Supporting Information Figure S1). The relatively high buffer gas pressure of about 10^{-3} mbar in the QIT MS results in collisional deactivation during the IR multiple-photon-excitation process, reducing the IRMPD efficiency for IR transitions with a small absorption cross section.[9,48] The effect is particularly noticeable for the dication because of its higher dissociation threshold as compared to the monocation. Experimental bond dissociation energies for the loss of a bpy unit from singly charged $M(bpy)_2^+$ were reported by Rodgers and co-workers[50−52] as 2.81 eV for Ni, 2.46 eV for Cu, and 2.33 eV for Zn. Our theoretical value of 2.43 eV for $[Cu(bpy)_2]^+$ is in good agreement, which gives confidence in the computed value for the dication of 5.27 eV.

In Figure 2b, the observed IRMPD spectrum for the monocation is seen to agree well with the theoretical spectrum, with the only exception being the deviation in the intensity of the band at 1155 cm^{-1}. The band assignments in the range from 1400 to 1700 cm^{-1} are analogous to those for the dication discussed above; bands in this region are mostly due to bpy ring vibrations and C−H in-plane bending. Similar also to the dication, the dominant IRMPD band at 754 cm^{-1} is due to C−H out-of-plane bending. A red shift of about 10 cm^{-1} is observed with respect to the dication. A similar 10 cm^{-1} red shift is observed for the IRMPD band at 1157 cm^{-1}, predicted also at 1157 cm^{-1}, due to the C−H in-plane bending. The band at 1307 cm^{-1} (C−H in-plane bending) remains unshifted as compared to the dication.

Figure 3 shows the optimized geometries of the two members of the $[Cu(bpy)_2]^{2+/+}$ redox pair. The excellent

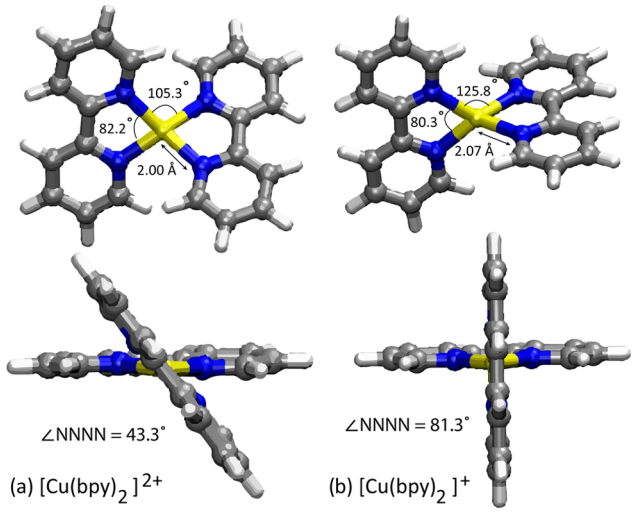

Figure 3. Computed structures of (a) $[Cu(bpy)_2]^{2+}$ as distorted square-planar coordination and (b) $[Cu(bpy)_2]^+$ as tetrahedral coordination.

agreement between the observed IR spectra and the computed ones allows a clear assignment of these structures. The geometry of the dication changes from distorted square-planar to tetrahedral upon charge reduction. Distortion from a pure square-planar configuration in the dication is likely due to steric repulsion between the two ligands. The tetrahedral configuration is indeed expected for the closed-shell Cu(I) ion. These observations indicate that thermalization of the monocation occurs after ETR inside the trap. Despite the available energy from the ETR reaction,[17,35,47] the monocation adopts its minimum energy structure and retains its tetradentate coordination, likely due to helium buffer gas cooling over the 200−250 ms duration of the ETR reaction.

The change in geometry upon charge reduction involves the change of the angle between the bpy ligands, in association with an increase of the average coordination bond lengths from 2.00 to 2.07 Å and intraligand angles (105.3−125.8°), while the ligand-bite angle (of the bpy moiety) is slightly decreased from 82 to 80° upon charge reduction (see Figure 3).

3.3. Mass Spectra of the $[Cu(cyclam)]^{2+/+}$ Redox Pair.

Figure 4 shows the mass spectrum obtained by ESI of a solution containing a Cu(II) salt and the macrocycle cyclam (1,4,8,11-tetra-azacyclotetradecane). The $[^{63}Cu(cyclam)]^{2+}$ isotopomer is observed at m/z 131.5 (see panel a and the zoom in panel b). This ion is mass-isolated in panel c for (i) charge reduction and (ii) recording of its IRMPD spectrum as a 2+ species. The charge reduction of this ion by ETR forms the $[^{63}Cu(cyclam)]^+$ ion at m/z 263 as indicated by the asterisk in panel d. In addition to charge reduction, the ETR of $[Cu(cyclam)]^{2+}$ ions also leads to ligand deprotonation, forming net singly charged ions as well, a process that is known from the common application of ETD in protein sequencing.[11,12,47,53] In fact, in the present experiment, the

DOI: 10.1021/acs.jpca.9b00793
J. Phys. Chem. A 2019, 123, 4149−4157

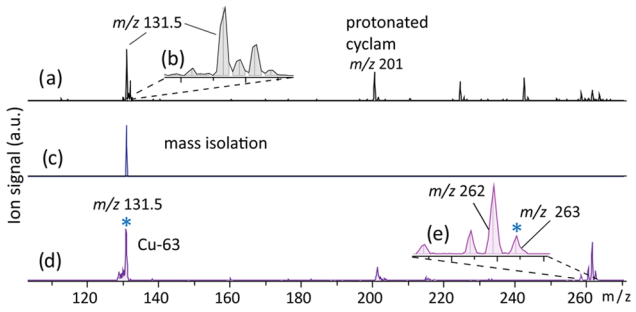

Figure 4. QIT ESI MS of a copper/cyclam solution (a) showing the $[^{63}Cu(cyclam)]^{2+}$ ion at m/z 131.5, with the isotope distribution of $[Cu(cyclam)]^{2+}$ ion zoomed in on in panel (b). Isotope-selective mass isolation of the $[^{63}Cu(cyclam)]^{2+}$ ion is shown in panel (c). ETR of isolated monoisotopic $[Cu(cyclam)]^{2+}$ in panel (d) shows the formation of the intact charge-reduced $[^{63}Cu(cyclam)]^{+}$ ion at m/z 263, with ETR-induced fragments at m/z 262, 261, and 258 attributed to the H, 2H, and 4H atom-loss products, respectively (see also zoom in on panel (e)). Members of the redox pair are indicated with blue stars.

MS/MS product ion resulting from ligand deprotonation (m/z 262) is the dominant ion in the MS (panels d and e). Note that the capability of the QIT MS to isolate a single Cu isotope of the 2+ precursor ion complex enables us to distinguish the one-electron reduction product from the deprotonation product[17] (e). Note also that in this case, we cannot generate the 1+ ion from the ESI directly, as was the case for the bis−bpy complex. Also, using a Cu(I) salt did not yield any appreciable amount of the 1+ coordination complex, so that the gas-phase ETR process is the only way to access the reduced form of the Cu(cyclam) complex.

3.4. IR Spectra and Structural Assignments. The complexes of Cu and cyclam can adopt different diastereomeric forms as shown in Scheme 1. The relative computed energies for these structures are listed in Table 1. Single-point

Table 1. Computed Relative Energies for Different Diastereomeric Complexes of $[Cu(cyclam)]^{+/2+}$ in kJ mol^{-1} at the B3LYP/6-31++G(d,p) and Single-Point MP2/6-311+G(d,p) Levels

	B3LYP/6-31++G(d,p)		sp-MP2/6-311+G(d,p)	
isomers	Cu^{2+}	Cu^{+}	Cu^{2+}	Cu^{+}
trans-I	10.8	3.1	6.2	14.4
trans-II	39.6	26.3	31.0	29.5
trans-III	0	1.5	0	16.9
trans-IV	68.2	50.6	67.0	55.2
trans-V	33.7	0	30.2	0

MP2/6-311+G(d,p) energies calculated at the B3LYP optimized geometries agree well with the energy ordering predicted by B3LYP/6-31++G(d,p) for the doubly charged complex. For the singly charged complex, the trans-I and trans-III structures are somewhat higher in energy relative to the trans-V minimum at the MP2 level as compared to the B3LYP level, and their relative ordering is reversed, although this is only a marginal difference. In the following discussion, we shall use the B3LYP energies.

In Figure 5, infrared spectra for the $[Cu(cyclam)]^{2+}$ ion and the charge-reduced $[Cu(cyclam)]^{+}$ ion are shown for comparison in the range of 500−1750 cm^{-1}. Both spectra share common features, although sensitive shifts of the vibrational bands are observed, indicating that the IR spectra are diagnostic for both species. Comparison with calculated spectra allows us to assign the vibrational normal modes and to derive which out of the five possible isomers (see Scheme 1) is present in the experiments for each member of the redox pair (vide infra).

3.4.1. [Cu(cyclam)]$^{2+}$. For the $[Cu(cyclam)]^{2+}$ ion, trans-III is the minimum-energy isomer (Figure 5), and the calculated harmonic IR spectrum indeed reproduces the experimental IR bands accurately. The next higher-energy isomer (+10.8 kJ mol^{-1}) is the trans-I isomer whose theoretical IR spectrum matches well with nearly all experimental bands, although the overall width of the intense unresolved feature near 1000 cm^{-1} is slightly better reproduced by the global minimum energy structure. The remaining diastereomers trans-II, trans-IV and trans-V are at least 30 kJ mol^{-1} higher in energy. Moreover, their computed spectra deviate more significantly from the experimental spectrum, particularly in the ranges 750−950 and 1150−1350 cm^{-1}, where several weaker bands (though probably not below the observation threshold) are predicted but not observed experimentally.

We assign the vibrational normal modes for the dication $[Cu(cyclam)]^{2+}$ on the basis of the computed spectrum for the global minimum trans-III isomer. The high-frequency bands between 1400 and 1500 cm^{-1} are attributed to the CH_2 and NH bending vibrations. The most intense feature centered at 1019 cm^{-1} is relatively broad and accommodates multiple unresolved transitions, particularly the C−N and C−C stretching modes, as well as N−H rocking modes. The low-intensity IRMPD bands at 1300 and 878 cm^{-1}, which remain unobserved in the QIT MS (see Figure 5), presumably due to collisional deactivation,[9,17,48] correspond to the predicted bands at 1320 and 868 cm^{-1}, respectively, which are due to the CH_2 twist and CH_2 rocking vibrations.

3.4.2. [Cu(cyclam)]$^{+}$. The IRMPD spectrum of the charge-reduced $[Cu(cyclam)]^{+}$ ion is dominated by three intense bands near 1070, 1422, and 1457 cm^{-1} as well as some lower-intensity bands at 822, 928, and 1340 cm^{-1} (see panels on the right in Figure 5). The trans-V isomer is the lowest-energy isomer for the complex in this charge state, and its theoretical IR spectrum reproduces all features in the experimental spectrum, except for predicted bands at 1167 and 970 cm^{-1}, which are not observed; admittedly, these bands are relatively weak and could be below an IRMPD cutoff. The next higher-energy isomer, trans-III, lies at only +1.5 kJ mol^{-1}. Its predicted IR spectrum matches well with the experimental one, even if no or only a very low cutoff is assumed, in agreement with the low dissociation threshold of this species. A small deviation is observed in the splitting of the weak bands just above 900 cm^{-1}, which is slightly larger in the computation than in the experiment. One may therefore argue that the silent range between 1100 and 1400 cm^{-1} is predicted better by trans-III than by trans-V. Based on the calculated spectrum for trans-III, we attribute the bands at 822 and 928 cm^{-1} to the CH_2 rocking modes. The highest frequency band at 1422 and 1457 cm^{-1} is due to coupled CH_2 bending and NH bending. The low-intensity band at 1340 cm^{-1} is due to CH_2 wagging.

The next higher-energy isomer is trans-I at +3.1 kJ mol^{-1}, which features two IR bands between 1200 and 1300 cm^{-1} in its predicted spectrum that are absent in the experiment. Also, the remaining isomers, which are substantially higher in energy (>25 kJ mol^{-1}), have predicted IR spectra that clearly deviate

DOI: 10.1021/acs.jpca.9b00793
J. Phys. Chem. A 2019, 123, 4149−4157

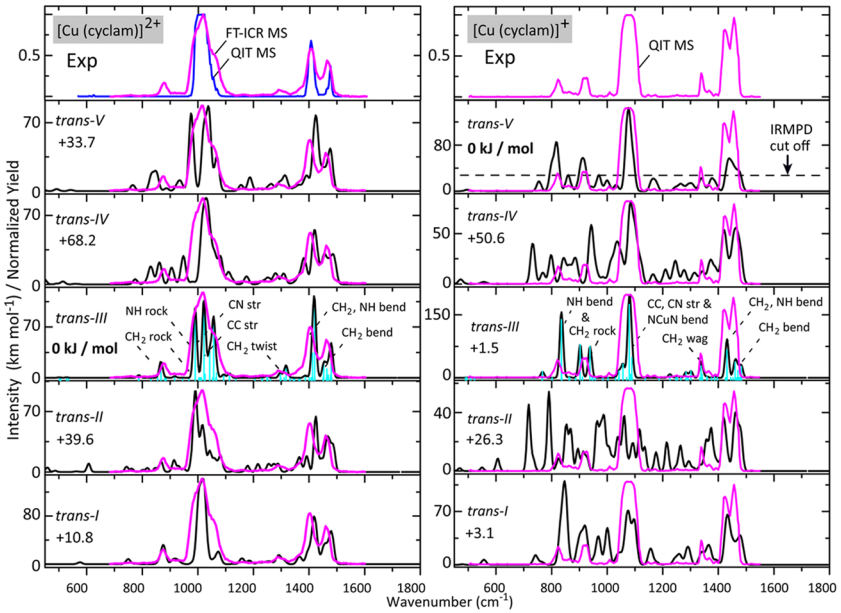

Figure 5. Experimental IRMPD spectrum of $[Cu(cyclam)]^{2+}$ recorded in the QIT MS (blue trace in the top left panel) and in the FTICR MS (magenta trace; left panels) and of the charge-reduced $[Cu(cyclam)]^{+}$ ion recorded in the QIT MS (magenta trace in the right panels). Experimental spectra are overlaid with the theoretical IR spectra computed for the five diastereomers shown in Scheme 1. Relative Gibbs free energies in kJ mol^{-1} are given in each panel. trans-III is the minimum energy structure for the dication, while trans-V is the lowest for the monocation, although trans-III is nearly isoenergetic for the 1+ species. All optimized structures are shown in Supporting Information Figure S2.

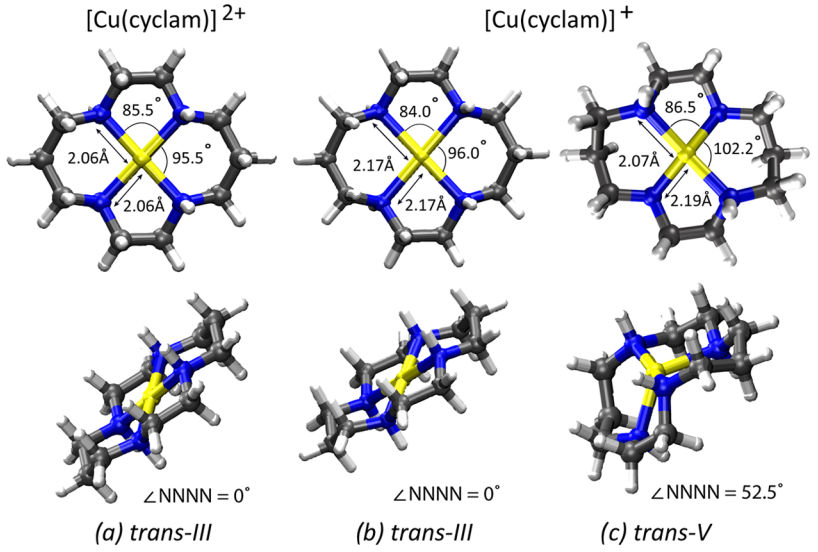

Figure 6. DFT-computed minimum-energy structures of (a) the trans-III isomer of $[Cu(cyclam)]^{2+}$, (b) the trans-III, and (c) trans-V isomers of $[Cu(cyclam)]^{+}$. The four nitrogen atoms of the cyclam ligand scaffold remain square planar of the trans-III isomer for both the dication and monocation, whereas a distorted tetrahedral coordination is possible for the trans-V isomer.

from the experiment. These diastereomers can safely be excluded to occur in the ion population.

In conclusion, for the dication complex, we assign the trans-III isomer. The experiments suggest that charge reduction of this species in the trap retains the stereoisomerism, so that the 1+ complex is also in the trans-III form, although a contribution from the trans-V form cannot be entirely excluded. Isomerization to trans-V would involve the breaking of the two Cu−N coordination bonds to allow for the inversion of the respective amine groups, followed by the restoration of the coordination bonds. We suspect that the energy cost of breaking the coordination bonds is too high, so this isomerization does not occur. We speculate that although the charge-recombination process may release a significant amount of energy virtually instantaneously, subsequent cooling by the buffer gas inside the trap outcompetes possible isomerization.

3.5. Structural Trend upon Charge Reduction. Figure 6 summarizes the relevant structural parameters of the two members of the Cu[cyclam] redox pair. Based on the good agreement between theoretical and experimental IR spectra, the isomeric form of the ligands can be confidently determined down to one or two diastereomers. From this assignment, we infer that isomerization is unlikely upon charge reduction of the gaseous $[Cu(cyclam)]^{2+}$ inside the QIT MS.

DOI: 10.1021/acs.jpca.9b00793
J. Phys. Chem. A 2019, 123, 4149−4157

In the dicationic complexes, copper has a $3d^9$ electron configuration, while after charge reduction, the 3d shell is filled ($3d^{10}$). One expects that the nature of the binding changes from orbital interaction driven to merely electrostatic binding, with ligand field effects being minimized.[33] Indeed, for the $Cu(bpy)_2$ complexes, this is reflected in the conversion of the nearly square-planar coordination of the Cu^{2+} center to a tetrahedral coordination around the closed-shell Cu^{1+} metal center. However, for the Cu(cyclam) complex, charge reduction leads merely to a slight increase of the Cu−N bond lengths, but conversion to a tetrahedral geometry is not observed in the computed structure for the trans-III isomer (see Figure 6). We attribute this to the strain in the macrocycle scaffold imposed by the relative orientations of the NH groups. In the trans-III isomer, two pairs of adjacent NH groups have the same orientation with respect to the plane of the complex; in the trans-V isomer, two opposite NH groups have the same orientation, and this allows for a coordination geometry that is closer to a tetrahedral (see Figure 6). Indeed, the trans-V isomer is computed to be lowest in energy. The spectroscopic data presented in Figure 5 suggest, however, that conversion to the trans-V isomer, and hence to tetrahedral coordination, is not achieved for Cu(cyclam), likely because of the high energetic barriers involved in the breaking of the Cu−N coordination bonds.

An interesting observation is that Ni^+(cyclam) and Cu^{2+}(cyclam) are isoelectronic, both metal ions possess a $3d^9$ electronic configuration. Since the ionic radius decreases from left to right in the periodic table, we indeed observe that the metal−ligand bond distance (M^{n+}−N) decreases by 0.04 Å for Cu^{2+}(cyclam) relative to Ni^+(cyclam), see Table 2.[17] On the other hand, upon charge reduction, the metal−ligand bond distance increases significantly for both metal ions. UV absorption spectroscopy and electrochemical study in a solution suggested that Cu(II) ion is bigger than Ni(II).[23,24] The same is true for the gas phase, where the metal−ligand distance increases for Cu^{2+}(cyclam) relative to that for Ni^{2+}(cyclam).

Table 2. Mean Bond Distances (in Å) from the DFT-Optimized Minimum-Energy Conformers of the Reduced and Oxidized Ions of [Ni/Cu(cyclam)][a]

trans-III		trans-III		trans-V[b]
Ni^{2+}−N	Ni^+−N	Cu^{2+}−N	Cu^+−N	Cu^+−N
1.98(0)	2.10(0)	2.06(0.01)	2.17(0)	2.07(0) and 2.19(0)

[a]Parenthesized values are the standard deviations. [b]Distorted tetrahedral conformer where the space diagonal nitrogen pair has unequal distances (diagonal NN): 3.82 versus 4.08 Å and angles (diagonal ∠NCuN): 121.4 versus 162.2°, respectively, while having a copper ion in the middle (see Figure 6) of both diagonal distances.

4. CONCLUSIONS

Two copper ligand complexes were spectroscopically investigated in both their 1+ and 2+ charge states to gain further insight into the gaseous electron-transfer reduction of transition-metal−ligand complexes and characterization of both members of the redox pair by IRMPD spectroscopy. The charge-reduced $[Cu(bpy)_2]^+$ ion was generated from its mass-isolated oxidized counterpart, the $[Cu(bpy)_2]^{2+}$ ion. The identical 1+ ion was also generated directly from the electrospray ionization source. IRMPD spectra of the singly charged $[Cu(bpy)_2]^+$ ion were found to be virtually identical irrespective of the source of the ions. This indicates that charge reduction in the gas phase by ETR can be followed by rapid thermalization, removing the energy released by the exothermic ETR reaction and allowing the 1+ complex to adopt its minimum-energy tetrahedral coordination geometry. The conversion from square-planar to tetrahedral coordination is indeed what is expected upon reduction of the metal center from d^9 to d^{10}. Note that the distortion from the ideal square-planar geometry for the $[Cu(bpy)_2]^{2+}$ ion is due to the steric repulsion of CH groups on the two bpy moieties.

The singly-charged $[Cu(cyclam)]^+$ ion is not formed by ESI, on account of the alkylamine nitrogens being harder Lewis bases than the pyridine nitrogens (and Cu^+ being a soft Lewis acid). The singly charged $[Cu(cyclam)]^+$ ion can therefore only be accessed by charge reduction of the mass-isolated dication, which uniquely allows us to record the IRMPD spectra of both members of the $[Cu(cyclam)]^{2+/+}$ redox pair. Theoretical investigations indicate that the minimum-energy isomers (diastereomers) for both charge states are different in the gas phase. However, comparison of theoretical results with the experiment suggests that isomerization is unlikely to occur upon charge reduction of the $[Cu(cyclam)]^{2+}$ ion. In contrast to the $Cu(bpy)_2$ system, the barrier to rearrangement is expected to be much higher, as it necessarily involves a temporary detachment of coordination bonds. Hence, we conclude that the ETR process in the QIT MS leaves the cyclam ligand intact and its coordination to the copper center unchanged. This is another indication of a rapid thermalization of the energy deposited into the system by the exothermic recombination reaction, attributed to collisional quenching with the helium buffer gas in the trap.

Finally, DFT is capable of identifying the structural changes and accurately explaining the structural trend for such complexes. ETR using the ETD option of the QIT MS combined with FEL-based IRMPD spectroscopy provides an interesting "gas-phase test tube" for probing redox reactions under isolated conditions.

■ ASSOCIATED CONTENT

Supporting Information

The Supporting Information is available free of charge on the ACS Publications website at DOI: 10.1021/acs.jpca.9b00793.

Experimental IRMPD spectrum for the $[Cu(bpy)_2]^{2+}$ ion recorded in the QIT MS at higher IR pulse energies to check for the presence of weak bands; DFT-optimized structures of [Cu(cyclam)] complexes for both members of the redox pair (PDF)

■ AUTHOR INFORMATION

Corresponding Author

*E-mail: joso@science.ru.nl.

ORCID

Jonathan Martens: 0000-0001-9537-4117
Giel Berden: 0000-0003-1500-922X
Jos Oomens: 0000-0002-2717-1278

Notes

The authors declare no competing financial interest.

DOI: 10.1021/acs.jpca.9b00793
J. Phys. Chem. A 2019, 123, 4149−4157

■ ACKNOWLEDGMENTS

We gratefully acknowledge the Nederlandse Organisatie voor Wetenschappelijk Onderzoek (NWO) for the support of the FELIX Laboratory and the FELIX staff for their assistance. Financial support for this project was provided by NWO Chemical Sciences under VICI project no. 724.011.002. We also thank NWO Physical Sciences (EW) and the SurfSARA Supercomputer Centre for providing the computational time and resources (grant 17603).

■ REFERENCES

(1) Rijs, A. M.; Oomens, J. *Gas-Phase IR Spectroscopy and Structure of Biological Molecules*; Springer, 2015; Vol. *364*.
(2) Polfer, N. C.; Oomens, J. Reaction Products in Mass Spectrometry Elucidated with Infrared Spectroscopy. *Phys. Chem. Chem. Phys.* **2007**, *9*, 3804−3817.
(3) Polfer, N. C.; Oomens, J. Vibrational Spectroscopy of Bare and Solvated Ionic Complexes of Biological Relevance. *Mass Spectrom. Rev.* **2009**, *28*, 468−494.
(4) Polfer, N. C. Infrared Multiple Photon Dissociation Spectroscopy of Trapped Ions. *Chem. Soc. Rev.* **2011**, *40*, 2211−2221.
(5) MacAleese, L.; Maitre, P. Infrared Spectroscopy of Organometallic Ions in the Gas Phase: From Model to Real World Complexes. *Mass Spectrom. Rev.* **2007**, *26*, 583−605.
(6) Eyler, J. R. Infrared Multiple Photon Dissociation Spectroscopy of Ions in Penning Traps. *Mass Spectrom. Rev.* **2009**, *28*, 448−467.
(7) Fridgen, T. D. Infrared Consequence Spectroscopy of Gaseous Protonated and Metal Ion Cationized Complexes. *Mass Spectrom. Rev.* **2009**, *28*, 586−607.
(8) Jašíková, L.; Roithová, J. Infrared Multiphoton Dissociation Spectroscopy with Free-Electron Lasers: On the Road from Small Molecules to Biomolecules. *Chem. - Eur. J.* **2018**, *24*, 3374−3390.
(9) Martens, J.; Berden, G.; Gebhardt, C. R.; Oomens, J. Infrared Ion Spectroscopy in a Modified Quadrupole Ion Trap Mass Spectrometer at the FELIX Free Electron Laser Laboratory. *Rev. Sci. Instrum.* **2016**, *87*, No. 103108.
(10) McLuckey, S. A.; Stephenson, J. L. Ion/Ion Chemistry of High-Mass Multiply Charged Ions. *Mass Spectrom. Rev.* **1998**, *17*, 369−407.
(11) Syka, J. E.; Coon, J. J.; Schroeder, M. J.; Shabanowitz, J.; Hunt, D. F. Peptide and Protein Sequence Analysis by Electron Transfer Dissociation Mass Spectrometry. *Proc. Natl. Acad. Sci. U.S.A.* **2004**, *101*, 9528−9533.
(12) Riley, N. M.; Coon, J. J. The Role of Electron Transfer Dissociation in Modern Proteomics. *Anal. Chem.* **2018**, *90*, 40−64.
(13) Coon, J. J. Collisions or Electrons? Protein Sequence Analysis in the 21st Century. *Anal. Chem.* **2009**, *81*, 3208−3215.
(14) Martens, J.; Grzetic, J.; Berden, G.; Oomens, J. Structural Identification of Electron Transfer Dissociation Products in Mass Spectrometry Using Infrared Ion Spectroscopy. *Nat. Commun.* **2016**, *7*, No. 11754.
(15) Kempkes, L. J.; Martens, J.; Berden, G.; Oomens, J. Spectroscopic Characterization of an Extensive Set of c-Type Peptide Fragment Ions Formed by Electron Transfer Dissociation Suggests Exclusive Formation of Amide Isomers. *J. Phys. Chem. Lett.* **2018**, *9*, 6404−6411.
(16) Kempkes, L. J.; Martens, J.; Berden, G.; Oomens, J. w-Type Ions Formed by Electron Transfer Dissociation of Cys-Containing Peptides Investigated by Infrared Ion Spectroscopy. *J. Mass Spectrom.* **2018**, *53*, 1207−1213.
(17) Munshi, M. U.; Craig, S. M.; Berden, G.; Martens, J.; DeBlase, A. F.; Foreman, D. J.; McLuckey, S. A.; Oomens, J.; Johnson, M. A. Preparation of Labile Ni^{+}(Cyclam) Cations in the Gas Phase Using Electron Transfer Reduction through Ion-Ion Recombination in an Ion Trap and Structural Characterization with Vibrational Spectroscopy. *J. Phys. Chem. Lett.* **2017**, *8*, 5047−5052.
(18) Billo, E. J.; Connolly, P. J.; Sardella, D. J.; Jasinski, J. P.; Butcher, R. J. Conformational Characterization of Square Planar Nickel (II) Tetraaza Macrocyclic Complexes by Proton NMR. Crystal Structure of [Ni (13aneN_4)] $ZnCl_4$. *Inorg. Chim. Acta* **1995**, *230*, 19−28.
(19) Cabbiness, D. K.; Margerum, D. W. Macrocyclic Effect on the Stability of Copper (II) Tetramine Complexes. *J. Am. Chem. Soc.* **1969**, *91*, 6540−6541.
(20) Busch, D. H. Distinctive Coordination Chemistry and Biological Significance of Complexes with Macrocyclic Ligands. *Acc. Chem. Res.* **1978**, *11*, 392−400.
(21) Martin, L. Y.; Sperati, C. R.; Busch, D. H. The Spectrochemical Properties of Tetragonal Complexes of High Spin Nickel (Ii) Containing Macrocyclic Ligands. *J. Am. Chem. Soc.* **1977**, *99*, 2968−2981.
(22) Hung, Y.; Martin, L. Y.; Jackels, S. C.; Tait, A. M.; Busch, D. H. Ring Size Effects among Metal Complexes with Macrocyclic Ligands: Synthesis, Stereochemistry, Spectrochemistry, and Electrochemistry of Cobalt (III) Complexes with Unsubstituted, Saturated Tetraaza Macrocycles. *J. Am. Chem. Soc.* **1977**, *99*, 4029−4039.
(23) Bhattacharya, P. Study of Cu (II) Complexes of Saturated Cyclic Tetra Amines. *J. Inorg. Nucl. Chem.* **1981**, *43*, 41−43.
(24) Barefield, E. K. Coordination Chemistry of N-Tetraalkylated Cyclam Ligands—a Status Report. *Coord. Chem. Rev.* **2010**, *254*, 1607−1627.
(25) Chan, M. K.; Mukund, S.; Kletzin, A.; Adams, M. W.; Rees, D. C. Ferredoxin Oxidoreductase. *Science* **1995**, *267*, 1463.
(26) Schindelin, H.; Kisker, C.; Hilton, J.; Rajagopalan, K.; Rees, D. C. Crystal Structure of DMSO Reductase: Redox-Linked Changes in Molybdopterin Coordination. *Science* **1996**, *272*, 1615−1621.
(27) Sorrell, T. N. Synthetic Models for Binuclear Copper Proteins. *Tetrahedron* **1989**, *45*, 3−68.
(28) Bol, J. *Synthetic Models for Dinuclear Copper Proteins*; University of Leiden, 1997.
(29) Dunbar, R. C.; Berden, G.; Martens, J. K.; Oomens, J. Divalent Metal-Ion Complexes with Dipeptide Ligands Having Phe and His Side-Chain Anchors: Effects of Sequence, Metal Ion, and Anchor. *J. Phys. Chem. A* **2015**, *119*, 9901−9909.
(30) Dunbar, R. C.; Martens, J.; Berden, G.; Oomens, J. Complexes of Ni (II) and Cu (II) with Small Peptides: Deciding Whether to Deprotonate. *Phys. Chem. Chem. Phys.* **2016**, *18*, 26923−26932.
(31) Dunbar, R. C.; Martens, J.; Berden, G.; Oomens, J. Transition Metal (II) Complexes of Histidine-Containing Tripeptides. Structures, and Infrared Spectroscopy by IRMPD. *Int. J. Mass Spectrom.* **2018**, *429*, 198−205.
(32) Anichini, A.; Fabbrizzi, L.; Paoletti, P.; Clay, R. M. A Microcalorimetric Study of the Macrocyclic Effect. Enthalpies of Formation of Copper (II) and Zinc (II) Complexes with Some Tetra-Aza Macrocyclic Ligands in Aqueous Solution. *J. Chem. Soc., Dalton Trans.* **1978**, *1978*, 577−583.
(33) Kaim, W.; Rall, J. Copper—a "Modern" Bioelement. *Angew. Chem., Int. Ed.* **1996**, *35*, 43−60.
(34) Hathaway, B.; Billing, D. The Electronic Properties and Stereochemistry of Mono-Nuclear Complexes of the Copper (II) Ion. *Coord. Chem. Rev.* **1970**, *5*, 143−207.
(35) Martens, J.; Berden, G.; Oomens, J. Structures of Fluoranthene Reagent Anions Used in Electron Transfer Dissociation and Proton Transfer Reaction Tandem Mass Spectrometry. *Anal. Chem.* **2016**, *88*, 6126−6129.
(36) Hartmer, R.; Kaplan, D. A.; Gebhardt, C. R.; Ledertheil, T.; Brekenfeld, A. Multiple Ion/Ion Reactions in the 3d Ion Trap: Selective Reagent Anion Production for ETD and PTR from a Single Compound. *Int. J. Mass Spectrom.* **2008**, *276*, 82−90.
(37) Chiavarino, B.; Crestoni, M. E.; Fornarini, S.; Taioli, S.; Mancini, I.; Tosi, P. Infrared Spectroscopy of Copper-Resveratrol Complexes: A Joint Experimental and Theoretical Study. *J. Chem. Phys.* **2012**, *137*, No. 024307.
(38) Pearson, R. G. Hard and Soft Acids and Bases. *J. Am. Chem. Soc.* **1963**, *85*, 3533−3539.
(39) Valle, J. J.; Eyler, J. R.; Oomens, J.; Moore, D. T.; Van Der Meer, A.; von Helden, G.; Meijer, G.; Hendrickson, C. L.; Marshall,

DOI: 10.1021/acs.jpca.9b00793
J. Phys. Chem. A 2019, 123, 4149−4157

A. G.; Blakney, G. T. Free Electron Laser-Fourier Transform Ion Cyclotron Resonance Mass Spectrometry Facility for Obtaining Infrared Multiphoton Dissociation Spectra of Gaseous Ions. *Rev. Sci. Instrum.* **2005**, *76*, No. 023103.
(40) Oomens, J.; Sartakov, B. G.; Meijer, G.; Von Helden, G. Gas-Phase Infrared Multiple Photon Dissociation Spectroscopy of Mass-Selected Molecular Ions. *Int. J. Mass Spectrom.* **2006**, *254*, 1−19.
(41) Almasian, M.; Grzetic, J.; van Maurik, J.; Steill, J. D.; Berden, G.; Ingemann, S.; Buma, W. J.; Oomens, J. Non-Equilibrium Isomer Distribution of the Gas-Phase Photoactive Yellow Protein Chromophore. *J. Phys. Chem. Lett.* **2012**, *3*, 2259−2263.
(42) Frisch, M. J.; Trucks, G. W.; Schlegel, H. B.; Scuseria, G. E.; Robb, M. A.; Cheeseman, J. R.; Scalmani, G.; Barone, V.; Mennucci, B.; Petersson, G. A.;et al.*Gaussian 09*, revision D.01; Gaussian, Inc.: Wallingford, CT, 2013.
(43) Becke, A. D. Density-Functional Thermochemistry. III. The Role of Exact Exchange. *J. Chem. Phys.* **1993**, *98*, 5648−5652.
(44) Becke, A. D. Becke's Three Parameter Hybrid Method Using the LYP Correlation Functional. *J. Chem. Phys.* **1993**, *98*, 5648−5652.
(45) Lee, C.; Yang, W.; Parr, R. G. Development of the Colle-Salvetti Correlation-Energy Formula into a Functional of the Electron Density. *Phys. Rev. B* **1988**, *37*, No. 785.
(46) Martens, J. K.; Grzetic, J.; Berden, G.; Oomens, J. Gas-Phase Conformations of Small Polyprolines and Their Fragment Ions by Irmpd Spectroscopy. *Int. J. Mass Spectrom.* **2015**, *377*, 179−187.
(47) Sobott, F.; Watt, S. J.; Smith, J.; Edelmann, M. J.; Kramer, H. B.; Kessler, B. M. Comparison of CID Versus ETD Based MS/MS Fragmentation for the Analysis of Protein Ubiquitination. *J. Am. Soc. Mass Spectrom.* **2009**, *20*, 1652−1659.
(48) Munshi, M. U.; Berden, G.; Martens, J. K.; Oomens, J. Gas-Phase Vibrational Spectroscopy of Triphenylamine: The Effect of Charge on Structure and Spectra. *Phys. Chem. Chem. Phys.* **2017**, *19*, 19881−19889.
(49) Nieckarz, R. J.; Oomens, J.; Berden, G.; Sagulenko, P.; Zenobi, R. Infrared Multiple Photon Dissociation (IRMPD) Spectroscopy of Oxazine Dyes. *Phys. Chem. Chem. Phys.* **2013**, *15*, 5049−5056.
(50) Rannulu, N. S.; Rodgers, M. Noncovalent Interactions of Zn^+ with N-Donor Ligands (Pyridine, 4, 4′-Dipyridyl, 2, 2′-Dipyridyl, and 1, 10-Phenanthroline): Collision-Induced Dissociation and Theoretical Studies. *J. Phys. Chem. A* **2012**, *116*, 1319−1332.
(51) Rannulu, N.; Rodgers, M. Noncovalent Interactions of Ni^+ with N-Donor Ligands (Pyridine, 4, 4′-Dipyridyl, 2, 2′-Dipyridyl, and 1, 10-Phenanthroline): Collision-Induced Dissociation and Theoretical Studies. *J. Phys. Chem. A* **2009**, *113*, 4534−4548.
(52) Rannulu, N. S.; Rodgers, M. T. Noncovalent Interactions of Cu^+ with N-Donor Ligands (Pyridine, 4,4-Dipyridyl, 2,2-Dipyridyl, and 1,10-Phenanthroline): Collision-Induced Dissociation and Theoretical Studies. *J. Phys. Chem. A* **2007**, *111*, 3465−3479.
(53) Graça, D. C.; Lescuyer, P.; Clerici, L.; Tsybin, Y. O.; Hartmer, R.; Meyer, M.; Samii, K.; Hochstrasser, D. F.; Scherl, A. Electron Transfer Dissociation Mass Spectrometry of Hemoglobin on Clinical Samples. *J. Am. Soc. Mass Spectrom.* **2012**, *23*, 1750−1756.

DOI: 10.1021/acs.jpca.9b00793
J. Phys. Chem. A 2019, 123, 4149−4157